HHS Public Access

Author manuscript

Mater Sci Eng A Struct Mater. Author manuscript; available in PMC 2021 January 07.

Published in final edited form as:

Mater Sci Eng A Struct Mater. 2020 January 7; 770: . doi:10.1016/j.msea.2019.138529.

The effects of alloying with Cu and Mn and thermal treatments on the mechanical instability of Zn-0.05Mg alloy

Morteza Shaker Ardakani, **Ehsan Mostaed**, **Malgorzata Sikora-Jasinska**, **Stephen L. Kampe**, **Jaroslaw W. Drelich**[1]

Department of Materials Science and Engineering, Michigan Technological University, Houghton, MI 49931, USA

Abstract

The detrimental effect of natural aging on mechanical properties of zinc alloys restricts their application as bioresorbable medical implants. In this study, aging of Zn-0.05Mg alloy and the effect of 0.5 Cu and 0.1 Mn (in weight percent) addition on the microstructure and tensile properties were studied. The alloys were cold rolled, aged and annealed; aiming to investigate the effects of precipitates and grain size on the mechanical properties and their stability. TEM analysis revealed that in ultrafine-grained binary Zn-0.05Mg alloy, the natural aging occurred due to the formation of nano-sized Mg_2Zn_{11} precipitates. After 90 days of natural aging, the yield strength and ultimate tensile strength of Zn-0.05Mg alloy increased from 197±4 MPa and 227±5 MPa to 233±8 MPa and 305±7 MPa, respectively, while the elongation was drastically reduced from 34±3% to 3±1%. This natural aging was retarded by adding the third element at either 0.1Mn or 0.5Cu quantities, which interacted with Mg in Zn solid solution and impeded the formation of Mg_2Zn_{11} precipitates. The addition of Cu and Mn elements increased alloy's strength, ductility, and its mechanical stability at a room temperature. The measured tensile strength and elongation were 274±5 MPa and 41±1% for Zn-0.1Mn-0.05Mg and 312±2 MPa and 44±2% for Zn-0.5Cu-0.05Mg, respectively. Annealing the alloys at elevated temperatures caused increase in both grain size and dissolution of secondary phases, and both affected alloy deformation mechanisms.

Keywords

Zn alloys; Natural aging; Mechanical properties; Grain refinement; Precipitation hardening

[1]Corresponding author: jwdrelic@mtu.edu.

Declaration of interests

The authors declare that they have no known competing financial interests or personal relationships that could have appeared to influence the work reported in this paper.

Data Availability Statement

The raw/processed data required to reproduce these findings cannot be shared at this time as the data also forms part of an ongoing study.

1. Introduction

Zinc (Zn) has shown promise as a bioresorbable medical material due to its appropriate corrosion rate and biocompatibility [1, 2]. However, inadequate mechanical strength of pure Zn impedes its application for vascular stenting applications. Extensive research has been conducted to tailor the mechanical properties of Zn through alloying elements and thermo-mechanical treatments [3–11]. Magnesium (Mg) has been used as an alloying element in many studies due to its well-known biocompatibility and a positive effect on the mechanical strength of Zn. Previous studies on Zn-Mg alloys demonstrated that increasing the Mg content consistently increases the tensile strength at the expense of the ductility due to the higher volume fraction of Mg_2Zn_{11} intermetallic [5, 12–15]. Recently, Zn-Mg alloys with Mg content below 0.1 wt.% were formulated to preserve zinc ductility [12, 16–19]. The tensile yield strength (TYS), ultimate tensile strength (UTS), and elongation for hot extruded Zn-0.05Mg alloy were reported as 160 MPa, 225 MPa, and 26%, respectively [16]. Jin et al. [17] reported the UTS and elongation values of 266 MPa and ~30%, respectively, for a cold drawn Zn-0.08Mg wire which could be ascribed to the higher Mg content and smaller grain sizes. The authors also reported a mechanical instability of the Zn-0.08Mg wire over time due to the room temperature aging, making the alloy unsuitable for bioresorbable stenting application. This aging behavior, which was attributed to the formation of brittle Mg_2Zn_{11} precipitates, depends on the diffusion rate of Mg solute. In general, Zn alloys age at room temperature due to diffusion at its relatively high homologous temperature [20]. This room temperature aging occurs more rapidly in Zn alloys containing a high density of grain boundaries, which act as high diffusion pathways [21].

To eliminate or at least hinder the natural aging process of Zn alloys, additional alloying elements need to be introduced. Based on results in the literature [22], it was hypothesized in an early stage of this project that both copper (Cu) and manganese (Mn) could be explored as additions to Zn-Mg alloys. In the ultrafine-grained Zn alloying systems containing Cu, room temperature dynamic precipitation dramatically increased the tensile elongation. The observed softening in tensile strength alongside room temperature superplastic ductility were attributed to the phase boundary sliding during the deformation. Therefore, precipitation in the Zn alloys containing additional elements at grain boundaries changed the deformation mechanism from dislocation-induced slipping to phase/grain boundary sliding. This could restore the ductility that resulted from the formation of the Mg-rich precipitates in the Zn-Mg based alloys. Third elements selected for this study have different solubilities in Zn; Mn with lower solubility (0.8 wt.% at 416°C) and Cu with higher solubility (2.75 wt.% at 425°C) [23].

In this study, the natural aging behavior of cold-rolled binary Zn-0.05Mg and ternary Zn-0.05Mg-X (X= 0.1Mn and 0.5Cu) alloys were studied over a period of 90 days. The characterization of the alloys included evolution of microstructure and changes in mechanical properties. In order to correlate the grain size and formation of precipitates to the mechanical properties of alloys, artificial aging and high temperature annealing were also performed on the rolled and naturally aged alloys, respectively.

2. Experimental procedures

In this study, pure Zn shot (99.99% purity- Alfa Aesar, Ward Hill, MA), Mg turnings (99.98% purity- Alfa Aesar), Mn powder (99.93% purity- Fisher Scientific, Pittsburgh, PA), and pure Cu shot (99.9% purity- Alfa Aesar) were used to formulate for melting. Three different alloys, listed in Table 1, were cast in sealed graphite crucibles at 700°C. The cast ingots, with diameter and length of 28 mm and 60 mm, respectively, were solution heat treated at 350 °C for 8h in air atmosphere furnace to homogenize the cast structure followed by water quenching.

The ingots were machined to a square rod with a 19×19mm cross-section. Multi-pass cold rolling was performed on the alloys to reduce their thickness to 0.60 mm. The dog-bone tensile samples with the gauge length and width of 12 mm and 3 mm, respectively, were cut from rolled sheet along the rolling direction using Japax wire electro-discharge machining (McWilliams EDM, Brighton, MI). Tensile testing was carried out on the investigated alloys prepared as follows:

- **i.** *Natural aging*: In order to investigate the natural aging behavior of the alloys, as-rolled samples were kept at room temperature for different times up to 90 days.
- **ii.** *Artificial aging*: The artificial aging behavior of Zn-0.5Cu-0.05Mg and Zn-0.1Mn-0.05Mg alloys at 80 °C for 6h to 96h was examined. However, for Zn-0.05Mg alloy, since it is strongly temperature sensitive, aging was conducted at a lower temperature of 50 °C for 12h to 24h. Furthermore, the aging behavior of Zn-0.05Mg alloy annealed at 320 °C for 30s was examined for aging times from 12h to 24h.
- **iii.** *Annealing*: The effect of grain size and precipitates on the tensile behavior of the naturally aged alloys were investigated. The annealing temperature was selected as 300 °C for Zn-0.5Cu-0.05Mg alloy and 320 °C for Zn-0.05Mg and Zn-0.1Mn-0.05Mg alloys. The tensile samples were annealed for a wide range of soaking times from 20s to 60s followed by water quenching.

Tensile properties of the alloys in as-rolled and after heat treatments in air atmosphere furnace were examined at the initial strain rate of 2×10^{-3} s^{-1} using an MTS HS72 mechanical testing machine (MTS, Eden Prairie, MN). The standard deviations were calculated from values obtained in each case from three tests. The fractured surface, and microstructure of samples, were characterized using a Philips XL 40 Environmental Scanning Electron Microscope (ESEM) (FEI, Hillsboro, OR) after standard mechanical polishing and etching with a 3% Nital solution (3 ml HNO_3 + 100 ml ethanol). The crystallographic texture of the selected samples was obtained using the electron backscattered diffraction (EBSD) analysis. The surface of the samples for the EBSD were prepared by standard mechanical polishing followed by low-angle Ar^+ ion milling for 15 minutes using voltage of 3.5 KV. The average grain sizes for all alloys were calculated by linear intercept method. Phase analysis was performed using X-ray diffraction (XRD) on a XDS-2000 θ-θ diffractometer (Scintag, Cupertino, CA) with CuKα radiation (Kα = 1.540562 Å) from 2θ = 35–90° at a speed of 0.01°/min with a step size of 0.02°. Additionally, naturally aged samples were analyzed by transmission electron microscopy

(TEM: Titan Themis S-TEM) (FEI, Hillsboro, OR) after reduction of the samples thickness to less than 100 μm followed by electro-polishing with 5 vol.% $HClO_4$ and 95 vol.% C_2H_5OH using voltage of 21 V at temperature of −25°C.

3. Results

3.1. Natural aging

The tensile stress-strain curves for the investigated alloys in the as-rolled condition are shown in the Fig. 1a and the tensile values are listed in Table 2. The Zn-0.05Mg alloy in as-rolled condition showed TYS, UTS and elongation of 197±4 MPa, 227±5MPa, and 34±3%, respectively. Addition of 0.1 wt% Mn to Zn-0.05Mg alloy not only increased the TYS and UTS to 230±3 MPa and 274±5 MPa, respectively, but also improved the elongation to fracture to 41±2% (Table 2). Similarly, in case of Cu-containing alloy, the TYS, UTS and ductility increased to 274±5 MPa, 312±2 MPa and 44±2%, respectively. The large amount of additional element prompted dislocation movement at higher stresses as compared to the Zn-0.05Mg alloy through solid solution and/or second phase strengthening and resulted in improved tensile strength [24].

Interestingly, natural aging effects were observed only for Zn-0.05Mg alloy (Fig. 1b), while the tensile properties of the ternary alloys remained unchanged during 90 days of their storage at room temperature. The tensile strength and ductility for Zn-0.05Mg alloy after 15, 30, and 90 days are listed in Table 2. With increasing the aging time up to 90 days, the UTS consistently increased from 227±5 MPa to 305±7 MPa, while the elongation dropped form 34±3% to 3±1%. Similarly, Jin et al. [17] reported an increase of UTS from 266 MPa to 434 MPa accompanied with a reduction of elongation from 30% to 3.5% for a massively cold worked Zn-0.08Mg wire after one year of storage at room temperature.

Fig. 2 shows that all of the investigated alloys in the as-rolled condition possess very fine microstructures due to the occurrence of dynamic recrystallization during the cold rolling. Pure Zn has a very low recrystallization temperature (around 10°C) [24]. Fig. 2a shows that Zn-0.05Mg alloy has a fully recrystallized fine equiaxed microstructure with the average grain size of 0.4±0.1 μm, while Zn-0.1Mn-0.05Mg alloy possesses a slightly larger grain size of 0.7±0.2 μm (Fig. 2b). The larger grain size for Zn-0.1Mn-0.05Mg alloy is due to the occurrence of grain growth in the absence of intermetallic particles which will be confirmed later by TEM microstructural studies. However, as seen in Fig. 2c, Zn-0.5Cu-0.05Mg alloy shows finer microstructure (average size of 0.5±0.1 μm) than the Mn-bearing alloy, resulting from particle pinning effect [25] accompanying with the particle stimulated nucleation regime [26] which promotes the recrystallization. The room temperature solubility of additional elements in this study in Zn is negligible and thus, they likely form intermetallics during room temperature deformation [22, 23]. The average grain size of the investigated alloys remained unchanged after 90 days of storage at room temperature.

The XRD analysis on the naturally aged Zn-0.5Cu-0.05Mg alloy indicates the formation of ε-$CuZn_4$ intermetallic with small peak intensity at $2\theta = 43.5°$ (Fig. 3a). However, for Zn-0.05Mg and Zn-0.1Mn-0.05Mg alloys, the absence of peaks related to possible

intermetallic phases (Mg_2Zn_{11}, $MnZn_{13}$ [23]) is likely due to their low content, below the resolution limit of XRD.

The dark field (DF) TEM image of Zn-0.05Mg alloy after natural aging for 90 days is shown in Fig. 3b. The red arrows indicate, Mg_2Zn_{11} precipitates that form within the grains. Formation of these hard precipitates during the natural aging increases the tensile strength and decreases the ductility of the Zn-0.05Mg alloy. The high angle annular dark field (HAADF) STEM image of one precipitate and selected area energy dispersive X-ray spectroscopy (EDS) is shown in Fig. 3c–d. The area "A" contains 1.5±0.4 wt.% Mg whereas the area "B" does not show any peak for Mg.

Fig. 4a and 4c show TEM micrographs of Zn-0.1Mn-0.05Mg and Zn-0.5Cu-0.05Mg alloys, respectively. The absence of any secondary phases in Zn-0.1Mn-0.05Mg alloy implies that the addition of 0.1 wt% Mn hinders the formation of Mg-rich precipitates (Fig. 4a). However, as shown in Fig. 5b, the EDS elemental map of Zn-0.1Mn-0.05Mg alloy indicates the presence of Mn clusters within the grains. In case of Zn-0.5Cu-0.05Mg alloy, TEM studies reveal the formation of ε-$CuZn_4$ precipitates induced by cold rolling (white particles in Fig. 5c), which is consistent with the XRD results presented in Fig. 3a. Bright field TEM image of the grain interiors indicates the formation of Cu-rich clusters without any Mg-rich precipitates (Fig. 4d). Accordingly, the TEM microstructure of both ternary alloys indicates that retardation of the natural aging is as a result of the interruption in the Mg_2Zn_{11} precipitation.

The fractured surfaces of the investigated alloys are presented in Fig. 5. The fractured surface of as-rolled Zn-0.05Mg alloy (Fig. 5a) consists of cleavage planes and dimples, indicating a mixed ductile and brittle fracture mode. However, after 90 days of natural aging (Fig. 5b), the fracture surface of Zn-0.05Mg alloy presents a brittle fracture mode due to the presence of cleavage planes without any dimples. The fracture surface of Zn-0.1Mn-0.05Mg and Zn-0.5Cu-0.05Mg alloys after 90 days of storage are shown in Fig. 5c and 5d, respectively. It can be clearly seen that the presence of a large number of dimples suggests the occurrence of a ductile fracture for Zn-0.1Mn-0.05Mg and Zn-0.5Cu-0.05Mg alloys, in agreement with their higher ductility reported in Fig. 1a.

3.2. Artificial aging

In order to study the effect of grain size on the aging behavior of the Zn-Mg alloy, artificial aging of Zn-0.05Mg alloy was conducted at 50°C with two different grain sizes; the as-rolled alloy and the alloy annealed at 320°C for 30s, with average grain sizes of 0.4±0.1μm and 4.5±0.3 μm, respectively. The engineering stress-strain curves and tensile properties of the rolled and annealed Zn-0.05Mg alloy after artificial aging are shown in Fig. 6a and 6b, respectively, and all the derived tensile properties are listed in Table 3. Fig. 6a shows that for the Zn-0.05Mg alloy with finer structure, 12h of aging resulted in an increase of UTS by ~23% and a remarkable drop in elongation (~82%). For the annealed alloy after 12h aging, no changes in tensile properties were observed (Fig. 6b). The Mg-rich intermetallic did not form during the aging for 12h after annealing, as shown in Fig. 7c. Fig. 7a shows that 12h of aging of as rolled Zn-0.05Mg alloy resulted in the formation of Mg_2Zn_{11} intermetallic (indicated by white arrows). However, annealing induced grain growth decreased the rate of

diffusion for Mg atoms significantly due to the decreased grain boundary density, which serve as high diffusion pathways, and eventually, hindered the formation of secondary phases (Fig. 7c). Accordingly, the alloys' tensile properties remain unchanged (Fig. 6b and Table 3).

Fig. 6a and Table 3 indicate that continuation of aging for 24h of the rolled Zn-0.05Mg alloy, which leads to the coarsening of Mg_2Zn_{11} intermetallic particles, reduced the TYS and UTS from 215±5 MPa and 268±4 MPa to 128±3 MPa and 208±2 MPa, respectively. In contrast, 24h aging of the annealed Zn-0.05Mg alloy improved the UTS by about 75% (from 163±3 MPa to 284±2 MPa) (Fig. 6b) due to the formation of hard Mg intermetallic (Fig. 7d). The Mg-rich intermetallic particles tend to form along the grain boundaries as indicated by white arrows in Fig. 7d, while reducing the ductility by restricting dislocation movement and annihilation at the grain boundaries.

The results of natural aging of ternary alloys indicate that they are not susceptible to ambient temperature aging. Here, the artificial aging at 80°C was investigated to elucidate the effect of third element addition to aging respond of the Zn-Mg based alloys. The tensile properties of the artificially aged ternary alloys are listed in Table 4. For the Zn-0.1Mn-0.05Mg alloy, as seen in Fig. 8a, any aging time below 96h did not change the mechanical properties. The BSE image of the artificially aged Zn-0.1Mn-0.05Mg alloy after 96h is shown in Fig. 9b. The formation of very fine $Zn_{13}Mn$ and Mg_2Zn_{11} precipitates (shown by arrows) enhances the tensile strength from 274±5 MPa to 328±5 MPa. However, the elongation of the Zn-0.1Mn-0.05Mg alloy drops to 10%, which is mainly attributed to the formation of brittle Mg-rich precipitates. It was shown that both Mg and Mn solute remained in the Zn solid solution after rolling and natural aging (Fig. 4b and 9a). Here, artificial aging at 80°C provided the required energy for diffusion of solutes, and results in occurrence of aging after 96h.

For the artificially aged Zn-0.5Cu-0.05Mg alloy (Fig. 8b and Table 4), the first 12h of aging is accompanied with a drop in TYS along with an increase in UTS. It is hypothesized that the formation of Mg_2Zn_{11} (Fig. 4d) improved the tensile strength at the early stage of artificial aging. However, further aging caused an increase in fraction of ε-$CuZn_4$ precipitates at the grain boundaries (Fig. 9d vs Fig. 9c). Reduction in tensile strength and preservation of ductility (Fig. 8b and Table 4) suggest that there is a compromise between the formation of the Cu-rich and Mg-rich precipitates at the grain boundaries in Zn-0.5Cu-0.05Mg alloy. Compared to Mn-bearing alloy, the softening in Zn-0.5Cu-0.05Mg alloy is more distinct due to significantly higher fraction of $CuZn_4$ particles whose interfaces with the Zn matrix provide a higher contribution to sliding during the deformation [22] (Fig. 9b and 9d).

3.3. Annealing

The effect of the secondary phases on the tensile properties of the artificially aged alloys was shown in the section 3.2. In this section, the effect of secondary phases' fractions and grain size on the tensile behavior of naturally aged alloys were studied using a relatively high temperature annealing. The effect of annealing at 320°C for 20s to 60s on the tensile properties of the naturally aged Zn-0.05Mg and Zn-0.1Mn-0.05Mg alloys is shown in Fig.

10a and 10b, respectively. For Zn-0.5Cu-0.05Mg alloy, the annealing temperature was set at 300°C and the tensile curves are shown in Fig. 10c. The tensile values and grain size calculated from EBSD map are listed in Table 5.

Annealing of Zn-0.05Mg alloy caused the dissolution of Mg-rich precipitates and enhancement of ductility. Fig. 11a shows that annealing for 20s increased the grain size from 0.4±0.1 μm to 2.6±0.3 μm, which resulted in 35% drop in the tensile strength (Fig. 10a). However, the retained Mg-rich precipitates still restrict the ductility of the material to 4±1%. According to the Zn-Mg phase diagram [10], the maximum solubility of Mg in Zn at 320°C is ~0.05 wt.% and all of Mg_2Zn_{11} could be dissolved in Zn solid solution in the Zn-0.05Mg alloy. The secondary phases dissolved completely after 30s of annealing at the temperature of 320°C, boosting the ductility of alloy to 22±2% and enabling work hardening. A previous study demonstrated that the work softening in small grained Zn alloys is due to dynamic recovery and recrystallization during tensile [22]. It can be seen that the work softening starts to disappear after grain growth as less dislocation annihilation occurs. The grain size increased to 9.4±1.2 μm after 60s of annealing (Fig. 11b), and thereby, the strain hardening rate enhanced.

Fig. 10b shows that annealing of the Zn-0.1Mn-0.05Mg alloy at 320°C for 20s resulted in a drop in UTS and elongation values from 274±5 MPa and 41±1% to 206±3 MPa and 19±1%, respectively. Since Mg/Mn-rich precipitates were not observed in the microstructure, Mg solute remained in the Zn solid solution due to the interaction with Mn solute and clusters. Annealing caused a significant drop in tensile strength resulted from grain growth and dissolution of Mn cluster, whereas ductility dropped about 50%. The grain boundary area after 20s of annealing (average grain size of 1.0±0.1 μm) still enables dislocation annihilation which resulted in a work softening. The average grain size of Zn-0.1Mn-0.05Mg annealed for 60s was 4.1±0.4 μm (Fig. 11d). The work softening begins to disappear with increasing the grain size and eventually, replaced by a strain hardening from dislocation interaction with solutes and other dislocations.

After annealing the Zn-0.5Cu-0.05Mg alloy in 300°C for 20s, the UTS slightly increased to 325±5 MPa (Fig. 10c). It is hypothesized that the Cu-rich precipitates and clusters (Fig. 4c and 4d) dissolve in the early stage of annealing, improving the Zn-0.5Cu-0.05Mg alloy tensile strength. Fig. 12 shows that continuation of annealing leads to further dissolution of the Cu-rich precipitates and thus, reduction of their volume fraction. After 30s of annealing, all of the ε-$CuZn_4$ precipitates dissolved in the Zn matrix so that they were not visible in the BSE images (Fig. 12b). The tensile stress-strain curves show a drop in tensile strength of alloy due to grain growth accompanying with a distinct strain hardening behavior upon deformation.

4. Discussion

4.1. Mechanism of natural aging in Zn-0.05Mg

It is well-documented that the natural aging depends on the diffusion rate of solute atoms, which in turn is strongly accelerated with higher diffusion coefficients at the grain boundaries compared to volume diffusion [21]. Therefore, the higher grain boundary

density, which results from the ultrafine-grained structure observed in all investigated alloys (Fig. 2), facilitates the diffusion of solute atoms and makes natural aging more pronounced during the 90 days of aging. Mg-rich precipitates form during the hot deformation processes, while during cold deformation, a portion of Mg atoms remains in Zn solid solution. Thus, diffusion of Mg atoms from the Zn matrix causes the formation of the Mg_2Zn_{11} intermetallic precipitates during the natural aging. Formation of these very fine and dispersed precipitates in the Zn-0.05Mg alloy (Fig. 3b and c) increases the tensile strength along with a sharp drop in the elongation. The restoration of ductility after dissolution of Mg_2Zn_{11} intermetallic by annealing the Zn-0.05Mg alloy at 320°C confirms the negative effect of Mg-rich precipitates on the ductility of the Zn alloys.

The extensive cold metal working during stent manufacturing processes that involves tube drawing may result in a very fine-grained microstructure, with a high density of grain boundaries. Therefore, the natural aging of Zn alloy stents will be inevitable. This mechanical instability would be more pronounced after implantation of the stent inside the human body due to the elevated temperature (37 °C). The comparison of aging of the as-rolled and annealed Zn-0.05Mg alloy at 50°C, depicted in Fig. 6a and 6b, respectively, elucidates the effect of grain boundary density on the mechanical instability. The artificial aging of the annealed samples with an average grain size of 4.5±0.3 μm occurs in larger aging duration than that in its finer grained counterpart (0.4±0.1μm).

4.2. Effect of Mn/Cu addition on aging of Zn-0.05Mg

The tensile testing results indicate that addition of Mn or Cu to Zn-0.05Mg alloy successfully retards, for at least 90 days, the natural aging process. It is speculated that the interaction between Mg and Mn/Cu atoms in the solid solution slows down the diffusion of solute atoms and prevents the formation of Mg-rich precipitates, which suppresses the natural aging of alloy. A similar mechanism was found by other researchers in Al-Cu when alloyed with tin [27, 28]. The addition of Sn to Al-Cu alloy slows the natural aging as a result of stronger Sn-vacancy bonding energy and thereby, reducing the amount of vacancies. In the Zn-0.05Mg alloy, since the alloy contains a small concentration of Mg, it is hypothesized that the interaction of Mn/Cu with Mg will retain the Mg atoms in the Zn solid solution. The artificial aging of ternary alloys at 80 °C demonstrate that this interaction in Mn-bearing alloy is stronger than that in its Cu-containing counterpart (Fig. 8a and 8b). As such, in the Zn-0.5Cu-0.05Mg alloy after 12h of aging, the precipitation of Mg-rich particle improves the tensile strength, while in the Zn-0.1Mn-0.05Mg alloy the enhancement of strength occurred after 96h aging. In addition, the strain softening observed in the Zn-0.5Cu-0.05Mg alloy, due to the formation of ε-$CuZn_4$ precipitates and activation of phase boundary sliding [22], counterbalances the effect of Mg_2Zn_{11} precipitates on the loss of ductility.

It was found that the formation of Mg_2Zn_{11} particles has a detrimental effect on the ductility of Zn-Mg based alloys. However, previous research reported ductility enhancement in binary Zn-Cu and Zn-Mn alloys after a large amount of cold working [22, 29]. The improvement in elongation is attributed to the activation of Zn/strain-induced precipitates boundary sliding which is significantly higher than that on the Zn/Zn interface [22]. Fig. 8b indicates an

improvement of tensile strength with formation of Mg-rich precipitates at 12h of aging, while longer aging times (> 96h) has a reverse effect on the tensile strength which is ascribed to the formation of Cu-rich particles. On the other hand, the elongation of Mn-bearing alloy was significantly reduced after 96h aging at 80 °C (Fig. 8a). It is therefore speculated that the formation of Mn-rich precipitates was not enough to overcome the strengthening effect of Mg-rich particles. Therefore, it is concluded that only the Mg-rich precipitates has a negative effect on the elongation in Zn-Mg-based alloys.

4.3. Effect of grain size on strain softening of Zn alloys

The tensile curves of as rolled samples, shown in Fig. 1a, indicate a strain softening behavior which is attributed to the dynamic recovery and dislocation annihilation at grain boundaries which is favored in the ultrafine-grained structures. The room temperature strain softening was also observed in various ultrafine-grained Zn alloys in the literature [8, 22, 30, 31]. The annealing of the studied alloys (Fig. 10) revealed that strain softening could be suppressed by the grain growth. At longer annealing times the strain hardening becomes evident. Indeed, with increasing the grain size the dislocation annihilation at grain boundaries decreases and therefore, the interaction of dislocations with solutes and other dislocation enhances the flow stress with further deformation, causing strain hardening behavior.

5. Conclusions

In this study, the natural aging, tensile behavior, and microstructure of Zn-0.05Mg binary alloy were compared with Zn-0.05Mg-X ternary alloys (X= 0.1Mn and 0.5Cu) in different heat treatment conditions. Based on the obtained results, the following conclusions can be drawn:

- The microstructure of cold rolled alloys reveals submicron grains which occur due to dynamic recrystallization during the cold working. The resulting higher density of grain boundary accelerates the natural aging rate of Zn-0.05Mg alloy.
- TEM analysis on the binary Zn-0.05Mg alloy proves the formation of nano-sized Mg_2Zn_{11} precipitates after natural aging. These precipitates are responsible for the large increase in tensile strength and drop in ductility of the alloy during room temperature storage.
- The room temperature precipitation of Mg_2Zn_{11} particles in the binary Zn-Mg alloy is mainly affected by alloy grain size, occurring in ultrafine grained alloys.
- Addition of Mn and Cu results in suppression of natural aging due to the deceleration of Mg atom diffusion rate by the presence of solute atoms. Indeed, in Zn-Mg-based alloys consisting of low content of Mg, Cu/Mn interacts with Mg solutes and keep them in the solid solution.
- The Mn-bearing alloy seems to be less vulnerable to the artificial aging than the Zn-0.5Cu-0.05Mg alloy due to the lower Mn content.
- Short-time annealing on the as-rolled alloys could successfully suppress the strain softening behavior due to the less amount of dynamic recovery and dislocation annihilation at grain boundaries.

Acknowledgments

U.S. National Institute of Health – National Heart, Lung, and Blood Institute, Grant 1R01HL144739–01A1, and Michigan Tech College of Engineering, through Cross-Cutting Initiative funding, are acknowledged for funding this work.

The authors acknowledge the Applied Chemical and Morphological Analysis Laboratory at Michigan Tech for use of the instruments and staff assistance.

References

[1]. Bowen PK, Drelich J, Goldman J, Zinc exhibits ideal physiological corrosion behavior for bioabsorbable stents, Adv Mater 25(18) (2013) 2577–82. 10.1002/adma.201300226. [PubMed: 23495090]

[2]. Bowen PK, Guillory RJ 2nd, Shearier ER, Seitz JM, Drelich J, Bocks M, Zhao F, Goldman J, Metallic zinc exhibits optimal biocompatibility for bioabsorbable endovascular stents, Mater Sci Eng C Mater Biol Appl 56 (2015) 467–72. 10.1016/j.msec.2015.07.022. [PubMed: 26249616]

[3]. Bowen PK, Seitz JM, Guillory RJ 2nd, Braykovich JP, Zhao S, Goldman J, Drelich JW, Evaluation of wrought Zn-Al alloys (1, 3, and 5 wt % Al) through mechanical and in vivo testing for stent applications, J Biomed Mater Res B Appl Biomater 106(1) (2018) 245–258. 10.1002/jbm.b.33850. [PubMed: 28130871]

[4]. Zhao S, Seitz JM, Eifler R, Maier HJ, Guillory RJ 2nd, Earley EJ, Drelich A, Goldman J, Drelich JW, Zn-Li alloy after extrusion and drawing: Structural, mechanical characterization, and biodegradation in abdominal aorta of rat, Mater Sci Eng C Mater Biol Appl 76 (2017) 301–312. 10.1016/j.msec.2017.02.167. [PubMed: 28482531]

[5]. Mostaed E, Sikora-Jasinska M, Mostaed A, Loffredo S, Demir AG, Previtali B, Mantovani D, Beanland R, Vedani M, Novel Zn-based alloys for biodegradable stent applications: Design, development and in vitro degradation, J Mech Behav Biomed Mater 60 (2016) 581–602. 10.1016/j.jmbbm.2016.03.018. [PubMed: 27062241]

[6]. Tang Z, Niu J, Huang H, Zhang H, Pei J, Ou J, Yuan G, Potential biodegradable Zn-Cu binary alloys developed for cardiovascular implant applications, J Mech Behav Biomed Mater 72 (2017) 182–191. 10.1016/j.jmbbm.2017.05.013. [PubMed: 28499166]

[7]. Sikora-Jasinska M, Mostaed E, Mostaed A, Beanland R, Mantovani D, Vedani M, Fabrication, mechanical properties and in vitro degradation behavior of newly developed ZnAg alloys for degradable implant applications, Mater Sci Eng C Mater Biol Appl 77 (2017) 1170–1181. 10.1016/j.msec.2017.04.023. [PubMed: 28531993]

[8]. Bednarczyk W, Wątroba M, Kawałko J, Bała P, Can zinc alloys be strengthened by grain refinement? A critical evaluation of the processing of low-alloyed binary zinc alloys using ECAP, Materials Science and Engineering: A 748 (2019) 357–366. 10.1016/j.msea.2019.01.117.

[9]. Bowen PK, Shearier ER, Zhao S, Guillory RJ 2nd, Zhao F, Goldman J, Drelich JW, Biodegradable Metals for Cardiovascular Stents: from Clinical Concerns to Recent Zn-Alloys, Adv Healthc Mater 5(10) (2016) 1121–40. 10.1002/adhm.201501019. [PubMed: 27094868]

[10]. Mostaed E, Sikora-Jasinska M, Drelich JW, Vedani M, Zinc-based alloys for degradable vascular stent applications, Acta Biomater 71 (2018) 1–23. 10.1016/j.actbio.2018.03.005. [PubMed: 29530821]

[11]. Katarivas Levy G, Goldman J, Aghion E, The Prospects of Zinc as a Structural Material for Biodegradable Implants—A Review Paper, Metals 7(10) (2017) 402 10.3390/met7100402.

[12]. Wang L-Q, Ren Y-P, Sun S-N, Zhao H, Li S, Qin G-W, Microstructure, Mechanical Properties and Fracture Behavior of As-Extruded Zn–Mg Binary Alloys, Acta Metallurgica Sinica (English Letters) 30(10) (2017) 931–940. 10.1007/s40195-017-0585-4.

[13]. Vojtech D, Kubasek J, Serak J, Novak P, Mechanical and corrosion properties of newly developed biodegradable Zn-based alloys for bone fixation, Acta Biomater 7(9) (2011) 3515–22. 10.1016/j.actbio.2011.05.008. [PubMed: 21621017]

[14]. Jarzębska A, Bieda M, Kawałko J, Koprowski P, Rogal Ł, Chulist R, Kania B, Sztwiertnia K, Pachla W, Kulczyk M, Synergistic effect of Mg addition and hydrostatic extrusion on

microstructure and texture of biodegradable low-alloyed zinc, IOP Conference Series: Materials Science and Engineering 375 (2018). 10.1088/1757-899x/375/1/012008.

[15]. Katarivas Levy G, Leon A, Kafri A, Ventura Y, Drelich JW, Goldman J, Vago R, Aghion E, Evaluation of biodegradable Zn-1%Mg and Zn-1%Mg-0.5%Ca alloys for biomedical applications, J Mater Sci Mater Med 28(11) (2017) 174 10.1007/s10856-017-5973-9. [PubMed: 28956207]

[16]. Xiao C, Wang L, Ren Y, Sun S, Zhang E, Yan C, Liu Q, Sun X, Shou F, Duan J, Wang H, Qin G, Indirectly extruded biodegradable Zn-0.05wt%Mg alloy with improved strength and ductility: In vitro and in vivo studies, Journal of Materials Science & Technology 34(9) (2018) 1618–1627. 10.1016/j.jmst.2018.01.006.

[17]. Jin H, Zhao S, Guillory R, Bowen PK, Yin Z, Griebel A, Schaffer J, Earley EJ, Goldman J, Drelich JW, Novel high-strength, low-alloys Zn-Mg (<0.1wt% Mg) and their arterial biodegradation, Mater Sci Eng C Mater Biol Appl 84 (2018) 67–79. 10.1016/j.msec.2017.11.021. [PubMed: 29519445]

[18]. Wang L, He Y, Zhao H, Xie H, Li S, Ren Y, Qin G, Effect of cumulative strain on the microstructural and mechanical properties of Zn-0.02 wt%Mg alloy wires during room-temperature drawing process, Journal of Alloys and Compounds 740 (2018) 949–957. 10.1016/j.jallcom.2018.01.059.

[19]. Lin S, Wang Q, Yan X, Ran X, Wang L, Zhou JG, Hu T, Wang G, Mechanical properties, degradation behaviors and biocompatibility evaluation of a biodegradable Zn-Mg-Cu alloy for cardiovascular implants, Materials Letters 234 (2019) 294–297. 10.1016/j.matlet.2018.09.092.

[20]. Leis W, Kallien L, Ageing of zinc alloys, Int Foundry Res 64(1) (2011) 2–23.

[21]. Mishin Y, Herzig C, Grain boundary diffusion: recent progress and future research, Mat Sci Eng a-Struct 260(1–2) (1999) 55–71. 10.1016/S0921-5093(98)00978-2.

[22]. Mostaed E, Ardakani MS, Sikora-Jasinska M, Drelich JW, Precipitation induced room temperature superplasticity in Zn-Cu alloys, Materials Letters 244 (2019) 203–206. 10.1016/j.matlet.2019.02.084. [PubMed: 31871366]

[23]. Baker H, Okamoto HJAI, Materials Park, Ohio 44073-, USA, 501, ASM Handbook Vol. 3 Alloy Phase Diagrams, (1992).

[24]. Callister WD, Rethwisch DG, Materials Science and Engineering: An Introduction, Wiley2010.

[25]. Hillert M, Inhibition of grain growth by second-phase particles, Acta Metallurgica 36(12) (1988) 3177–3181. 10.1016/0001-6160(88)90053-3.

[26]. Robson JD, Henry DT, Davis B, Particle effects on recrystallization in magnesium–manganese alloys: Particle-stimulated nucleation, Acta Materialia 57(9) (2009) 2739–2747. 10.1016/j.actamat.2009.02.032.

[27]. Kimura H, Hasiguti RR, A General Treatment of the Distribution of Vacancies to Solute Atoms in a Ternary Solid Solution and its Application to Low Temperature Aging in Al–Cu–Sn Alloys, Transactions of the Japan Institute of Metals 16(6) (1975) 361–368. 10.2320/matertrans1960.16.361.

[28]. Kimura H, Hasiguti RK, Interaction of vacancies with Sn atoms and the rate of G-P zone formation in an Al-Cu-Sn alloy, Acta Metallurgica 9(12) (1961) 1076–1078. 10.1016/0001-6160(61)90179-1.

[29]. Shi ZZ, Yu J, Liu XF, Microalloyed Zn-Mn alloys: From extremely brittle to extraordinarily ductile at room temperature, Materials & Design 144 (2018) 343–352. 10.1016/j.matdes.2018.02.049.

[30]. Guo PS, Li FX, Yang LJ, Bagheri R, Zhang QK, Li BQ, Cho K, Song ZL, Sun WS, Liu HN, Ultra-fine-grained Zn-0.5Mn alloy processed by multi-pass hot extrusion: Grain refinement mechanism and room-temperature superplasticity, Mat Sci Eng a-Struct 748 (2019) 262–266. 10.1016/j.msea.2019.01.089.

[31]. Bednarczyk W, Kawałko J, Wątroba M, Bała P, Achieving room temperature superplasticity in the Zn-0.5Cu alloy processed via equal channel angular pressing, Materials Science and Engineering: A 723 (2018) 126–133. 10.1016/j.msea.2018.03.052

Research highlights

- Cold rolling resulted in the formation of an equiaxed ultrafine-grained structure for Zn-Mg-based alloys.
- Zn-0.05Mg alloy exhibited room temperature mechanical instability due to the formation of nanosized Mg_2Zn_{11} precipitates.
- Precipitation of Mg_2Zn_{11} particles was strongly influenced by grain size.
- Natural aging of Zn-0.05Mg was suppressed by addition of Cu and Mn elements due to their interaction with Mg solutes.
- Grain size had a significant contribution to the strain softening behavior of the samples during the tensile testing.

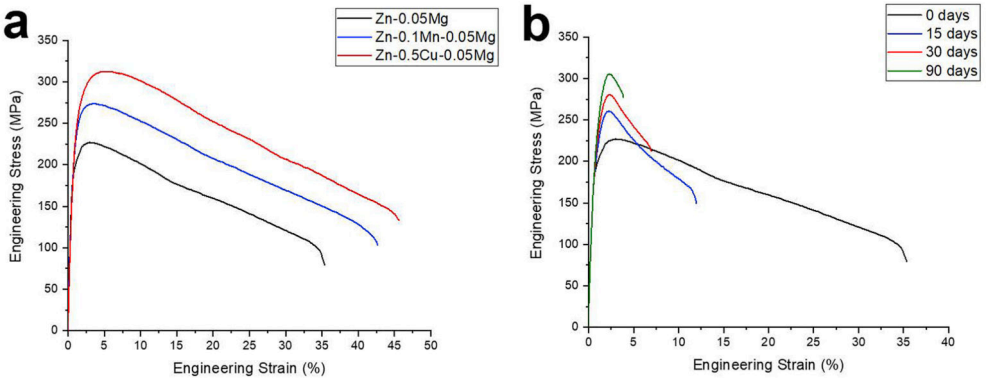

Fig. 1.

The stress-strain curve of a) investigated alloys in as-rolled condition, and b) Zn-0.05Mg alloy after different storage time at room temperature.

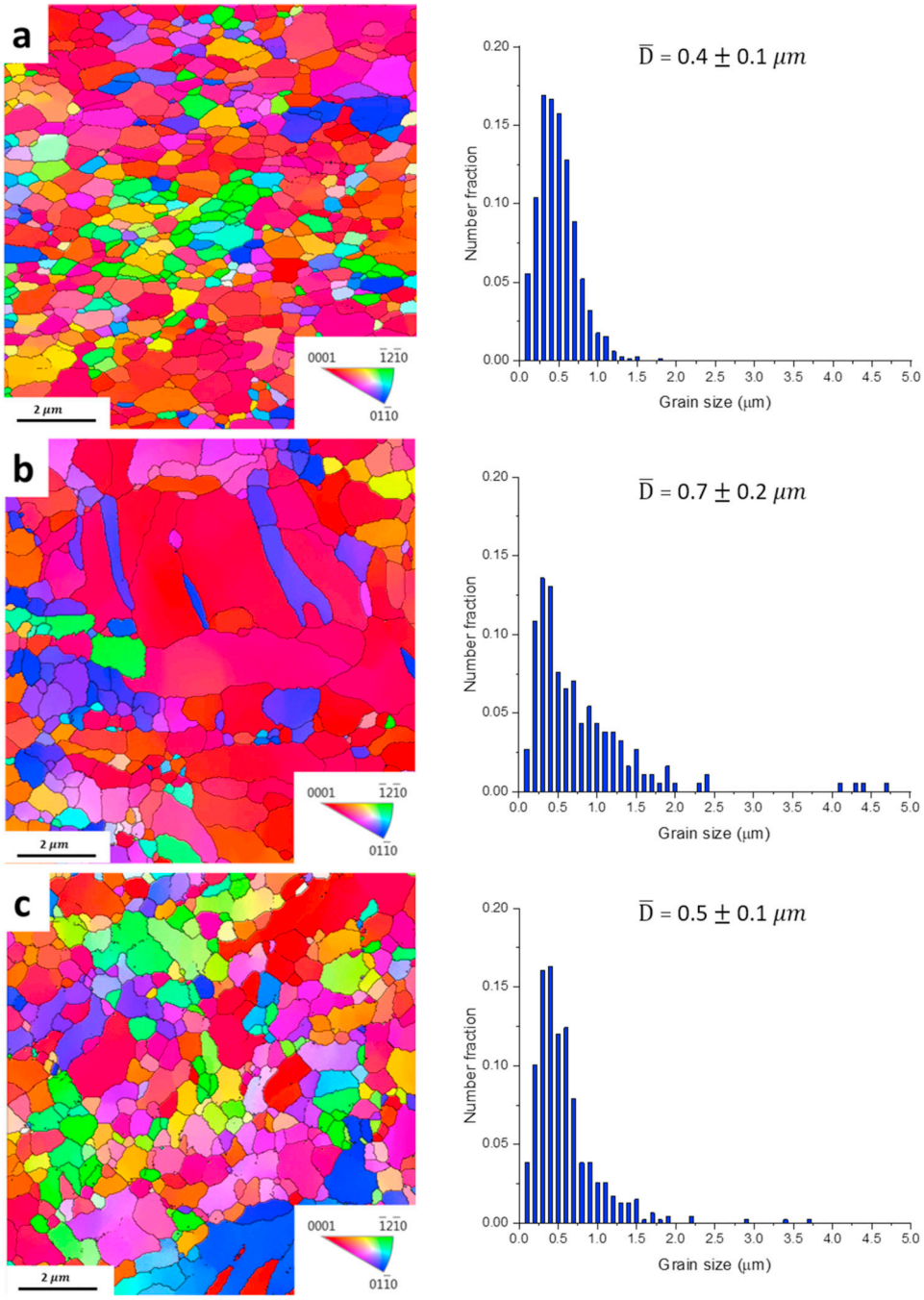

Fig. 2.

EBSD maps and the corresponding grain size distribution of as-rolled: a) Zn-0.05Mg, b) Zn-0.1Mn-0.05Mg, and c) Zn-0.5Cu-0.05Mg alloys.

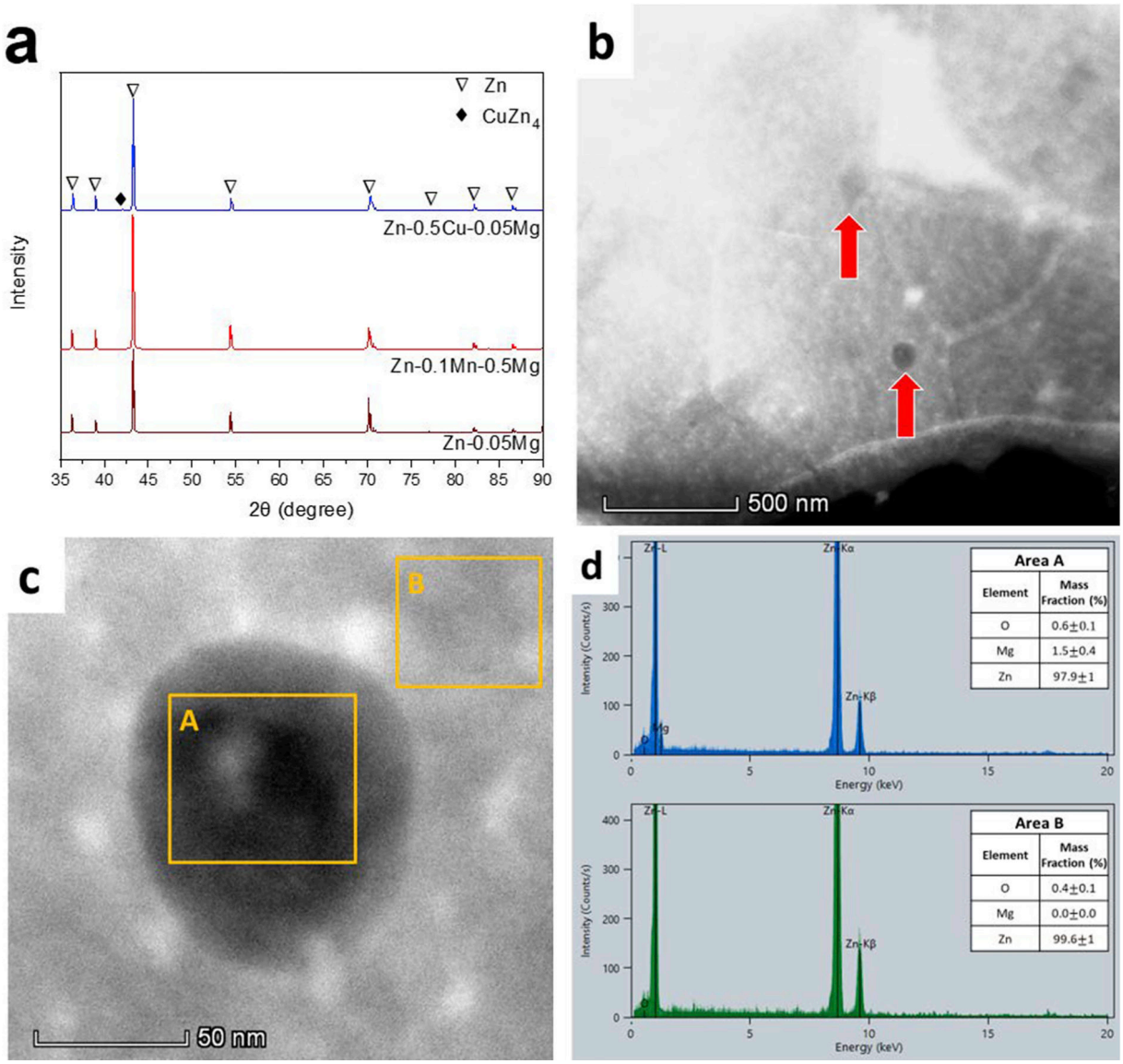

Fig. 3.

a) XRD patterns of the investigated alloys after 90 days of natural aging, b) DF TEM image of Zn-0.05Mg alloy, c) the HAADF-STEM image of the Mg-rich precipitate and Zn matrix and d) their corresponding EDS analyses.

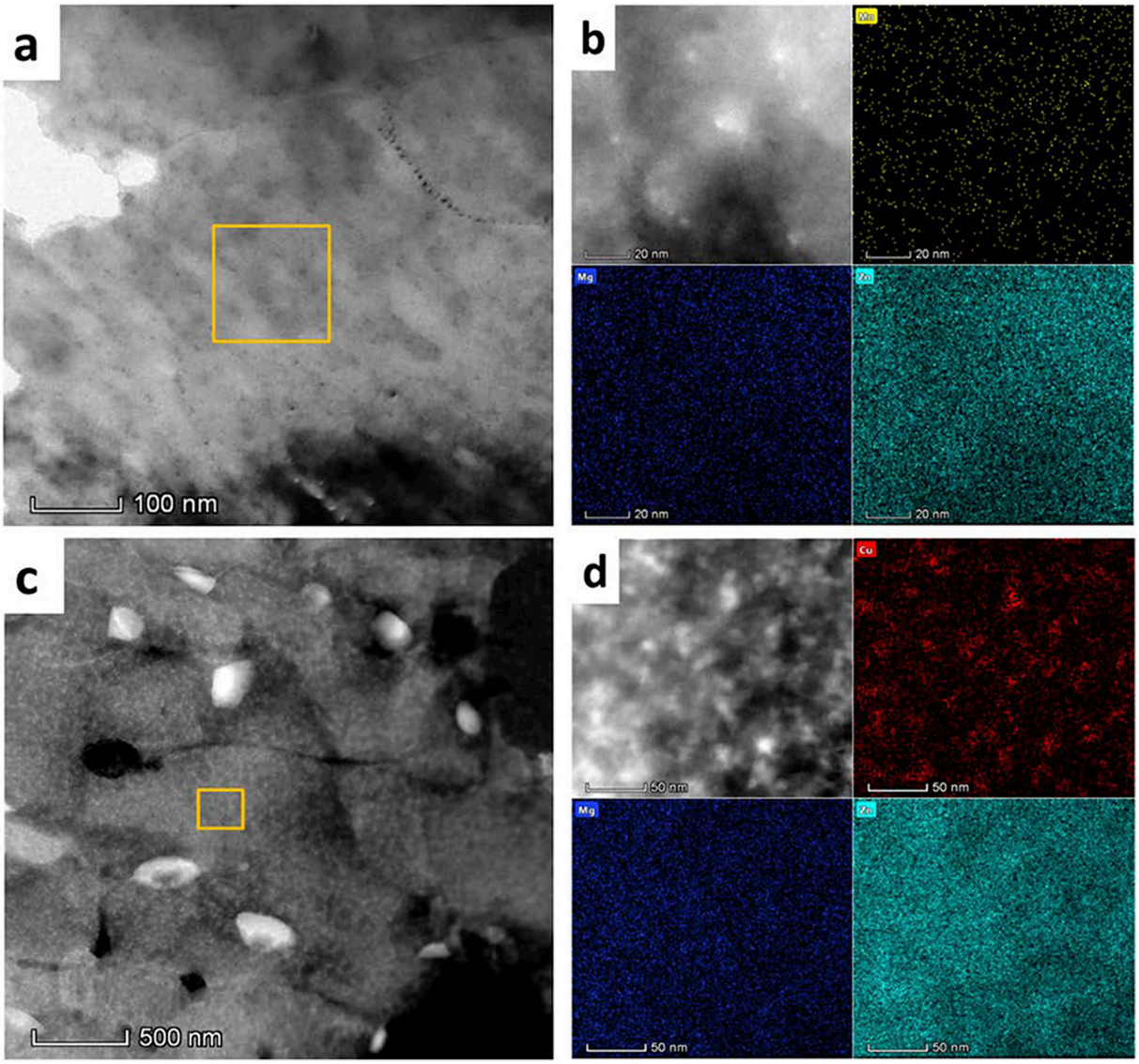

Fig. 4.

TEM image and HAADF-STEM image of selected area with their corresponding EDS elemental map for (a,b) Zn-0.1Mn-0.05Mg and (c-d) Zn-0.5Cu-0.05Mg alloys.

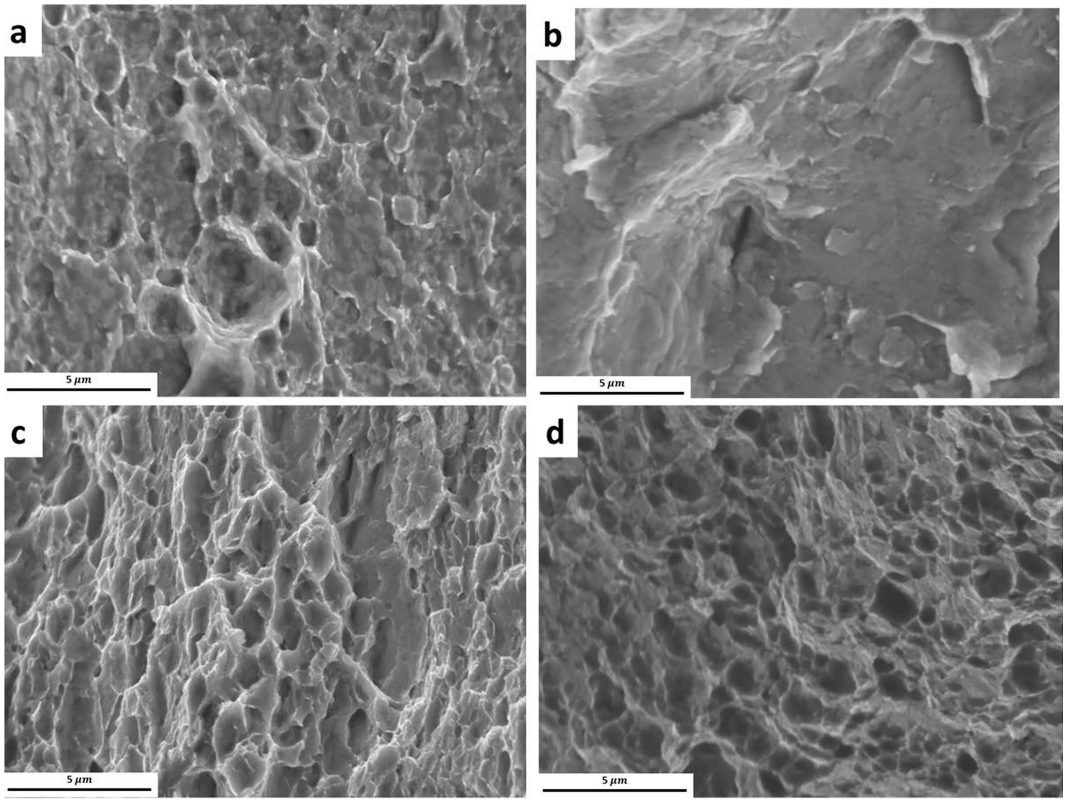

Fig. 5.

Fracture surface of (a, b) as-rolled and naturally aged Zn-0.05Mg alloy, respectively, c) Zn-0.1Mn-0.05Mg and d) Zn-0.5Cu-0.05Mg alloys after 90 days.

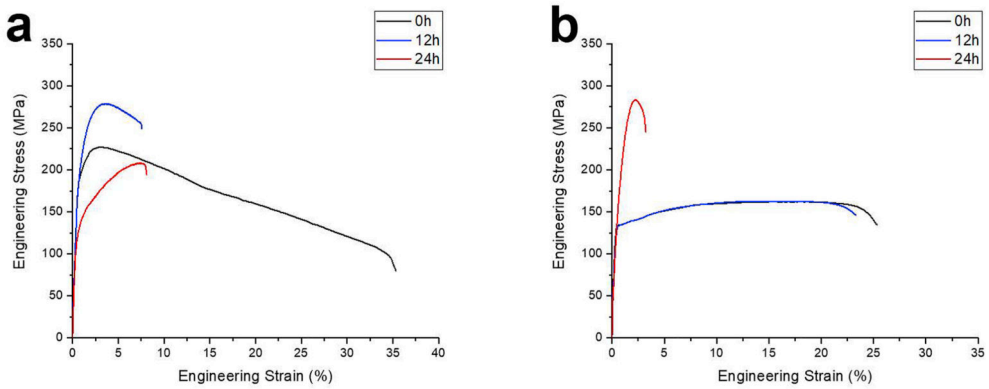

Fig. 6.

The stress-strain curve of aged Zn-0.05Mg alloy at 50°C a) after rolling, and b) after annealing at 320°C for 30s.

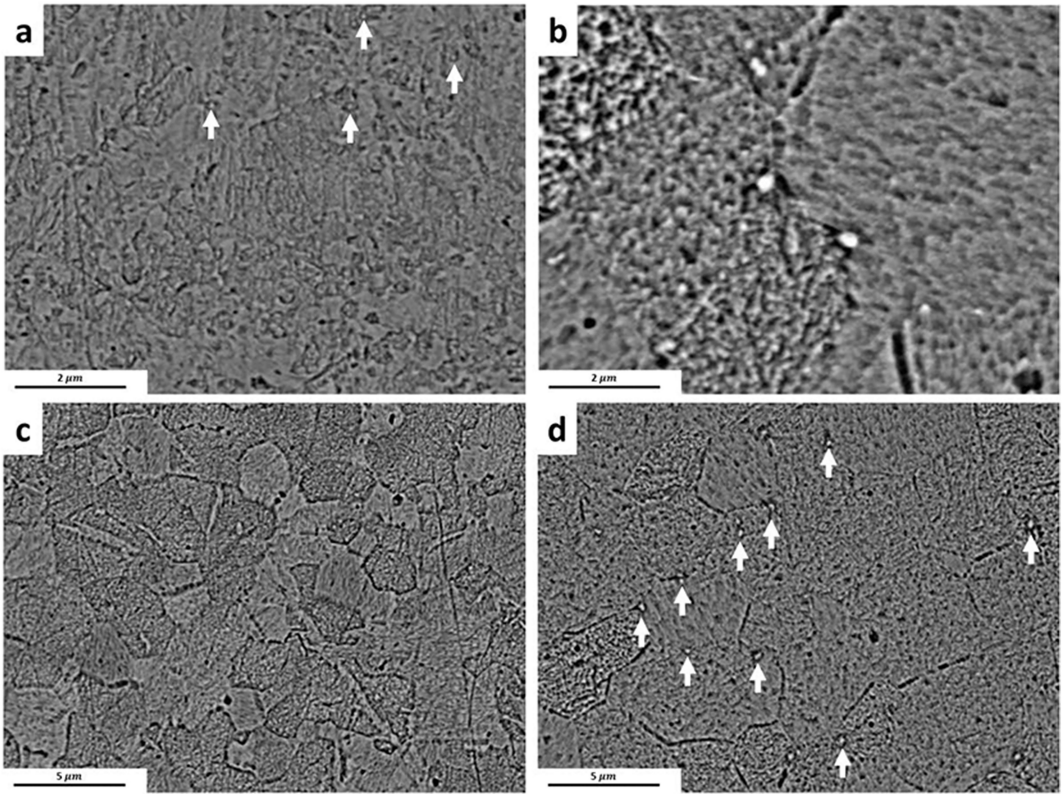

Fig. 7.

The BSE image of the Zn-0.05Mg alloy aged at 50°C for a) 12h and b) 24h after rolling; aged at 50°C for c) 12h and d) 24h after annealing at 320 °C for 30s.

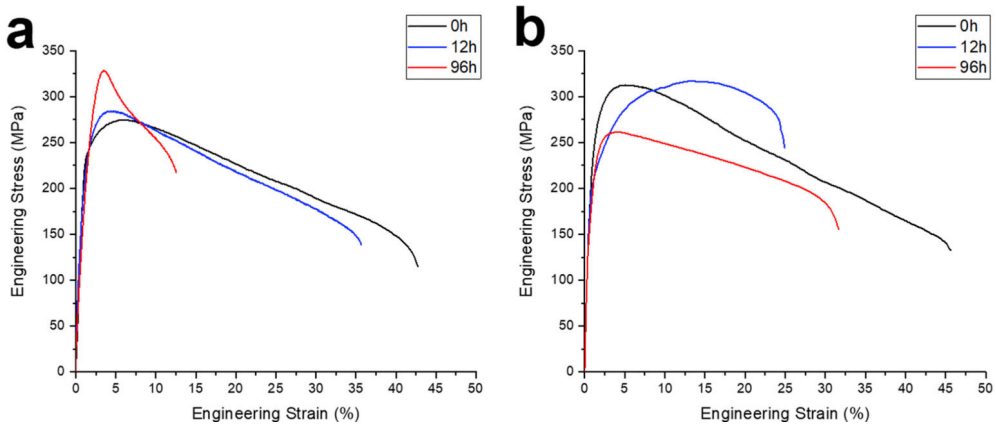

Fig. 8.

The stress-strain curves of a) Zn-0.1Mn-0.05Mg alloy and b) Zn-0.5Cu-0.05Mg alloy aged at 80°C.

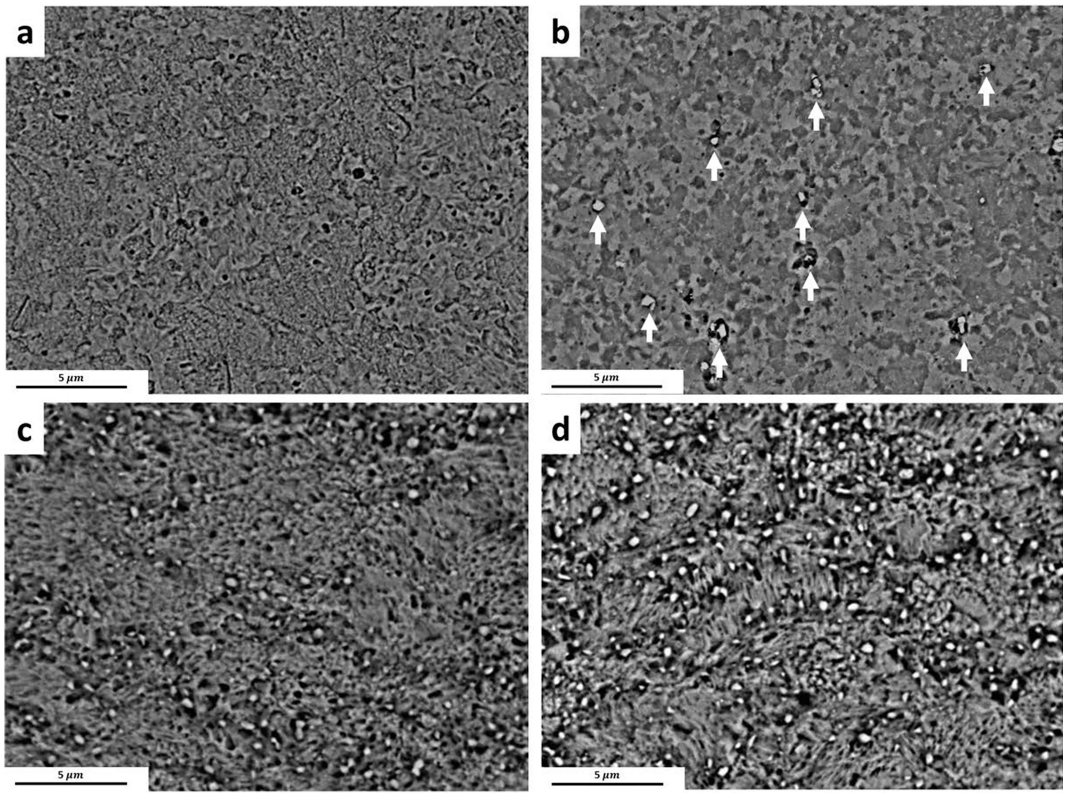

Figure 9-

The BSE image of as rolled and aged at 80°C for 96h of (a, b) Zn-0.1Mn-0.05Mg, and (c, d) Zn-0.5Cu-0.05Mg alloys, respectively.

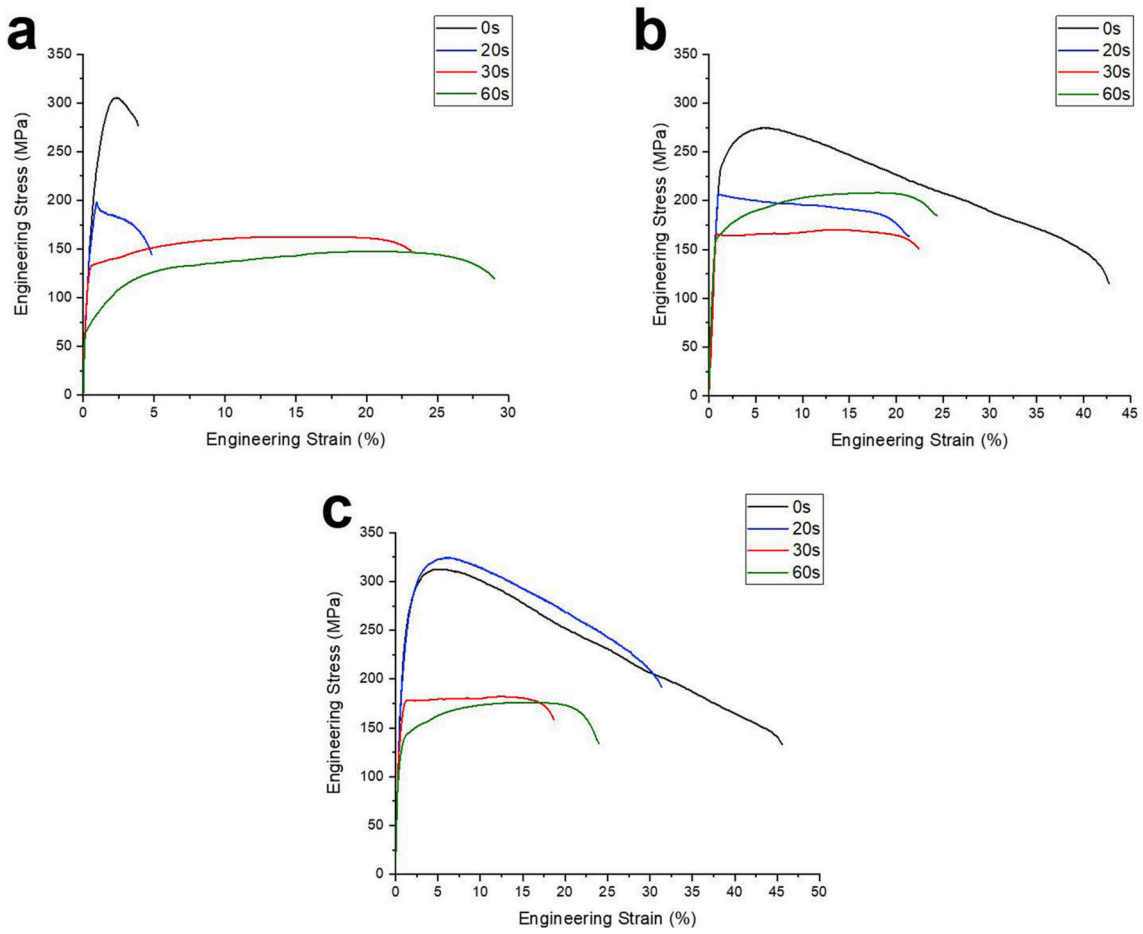

Fig. 10.

The stress-strain curves of annealed alloys up to 120s: a) Zn-0.05Mg at 320°C, b) Zn-0.1Mn-0.05Mg at 320°C, and C) Zn-0.5Cu-0.05Mg at 300°C.

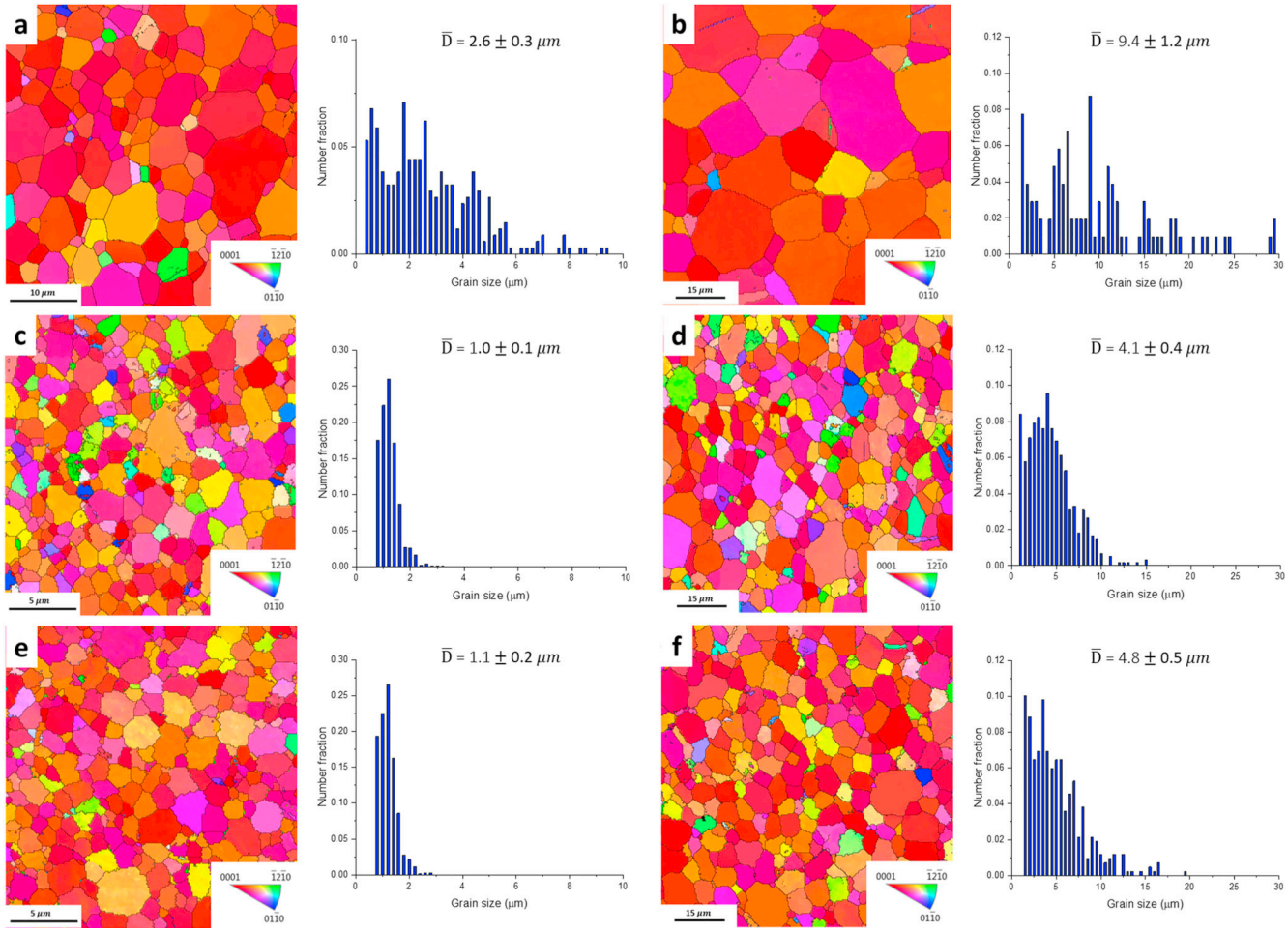

Fig. 11.

EBSD maps and the corresponding grain size distribution of the alloys after 20s (a, c and e) and 60s (b, d and f) of annealing; (a, b) Zn-0.05Mg, (c, d) Zn-0.1Mn-0.05Mg alloys after annealing at 320°C, and (e and f) Zn-0.5Cu-0.05Mg alloys annealed at 300°C.

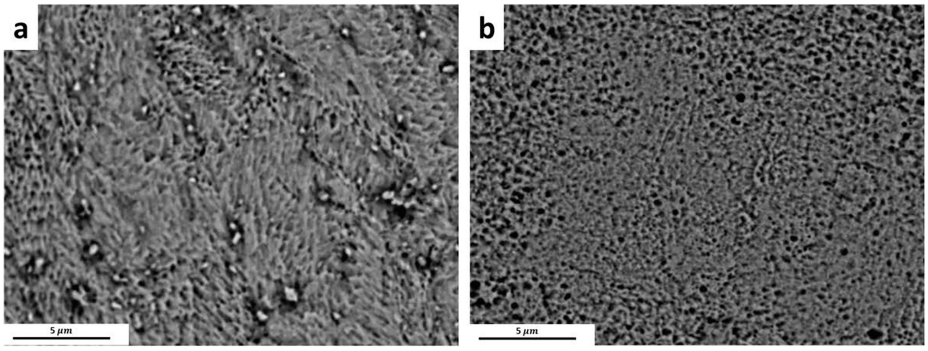

Fig. 12.
BSE image of Zn-0.5Cu-0.05Mg alloy annealed at 300°C for a) 20s, and b) 30s.

Table 1.

The nominal compositions of the investigated alloys.

Alloy	Mg (wt%)	Mn (wt%)	Cu (wt%)	Zn (wt%)
Zn-0.05Mg	0.05	0	0	Bal.
Zn-0.1Mn-0.05Mg	0.05	0.1	0	Bal.
Zn-0.5Cu-0.05Mg	0.05	0	0.5	Bal.

Table 2.

Mechanical properties of alloys studied in as rolled and naturally aged condition.

Alloy	Condition	TYS (MPa)	UTS (MPa)	Ductility (%)	Grain size (*μm*)
Zn-0.05Mg	As rolled	197±4	227±5	34±3	0.4±0.1
	Naturally aged 15 days	203±6	261±4	11±2	0.4±0.1
	Naturally aged 30 days	217±5	281±6	5±1	0.4±0.1
	Naturally aged 90 days	233±8	305±7	3±1	0.4±0.1
Zn-0.1Mn-0.05Mg	As rolled/ Naturally aged	230±3	274±5	41±1	0.7±0.2
Zn-0.5Cu-0.05Mg	As rolled/ Naturally aged	241±5	312±2	44±2	0.5±0.1

Table 3-

Mechanical properties of Zn-0.05Mg alloy aged at 50°C after rolling and annealing at 320°C for 30 seconds.

Condition	aging time (h)	TYS (MPa)	UTS (MPa)	Ductility (%)
Artificially aged at 50 °C	0	197±4	227±5	34±3
	6	215±5	268±4	20±2
	12	215±4	279±6	6±1
	24	128±3	208±2	7±1
Annealed at 320 °C **+ artificially aged at 50** °C	0	133±2	163±3	22±2
	12	134±3	162±3	24±2
	24	248±2	284±2	2±1
	48	168±4	250±4	5±1

Table 4.

Mechanical properties of artificially aged ternary alloys at 80 °C.

Alloy	Soaking time (h)	TYS (MPa)	UTS (MPa)	Ductility (%)
Zn-0.1Mn-0.05Mg	0	230±3	274±5	41±1
	12	250±7	284±4	34±1
	96	289±2	328±5	10±2
Zn-0.5Cu-0.05Mg	0	241±5	312±2	44±2
	12	208±3	317±5	23±2
	96	193±2	261±4	30±2

Table 5.

Mechanical properties of the 90-day stored alloys after different times of annealing.

Alloy	Temperature (°C)	Soaking time (s)	TYS (MPa)	UTS (MPa)	Ductility (%)	Grain size (μm)
Zn-0.05Mg	320	0	233±8	305±7	3±1	0.4±0.1
		20	189±6	198±5	4±1	2.6±0.3
		30	133±2	163±3	22±2	-
		60	65±2	148±6	28±3	9.4±1.2
Zn-0.1Mn-0.05Mg	320	0	230±3	274±5	41±1	0.7±0.2
		20	206±5	206±3	19±1	1.0±0.1
		30	164±3	170±6	21±3	-
		60	161±4	208±5	22±2	4.1±0.4
Zn-0.5Cu-0.05Mg	300	0	241±5	312±2	44±2	0.5±0.1
		20	241±3	325±5	30±2	1.1±0.2
		30	168±5	182±4	17±3	-
		60	129±8	176±2	22±2	4.8±0.5